

# On the distribution of magnetic null points above the solar photosphere

D.W. Longcope

*Department of Physics, Montana State University, Bozeman, Montana 59717*

D. S. Brown and E.R. Priest

*Department of Mathematics and Statistics, University of St. Andrews, St. Andrews KY16 9SS, UK*

(Dated: March 4, 2003)

Many theories predict magnetic energy dissipation at locations, called null points, where the magnetic field vanishes. In several astrophysical contexts, most notably the solar corona, energy is released within a low- $\beta$  magnetic field anchored to a lower boundary, the photosphere. We derive a general expression for the distribution of magnetic null points in potential magnetic fields anchored to a random, homogeneous distribution of field on the lower boundary. For all such fields the null point density decreases with height and scales with the inverse cube of the field's characteristic length. For photospheric fields which appear unipolar at the largest scales the nulls are confined to a narrow layer. We apply our results to models of the quiet Sun whose photospheric field consists of discrete sources of mixed polarity. The number of coronal nulls depends on the degree of imbalance between positive and negative sources. Numerical experiments reveal that the greatest column density of null points occurs when  $\sim 20\%$  of the sources are of the minority sign. Were the coronal energy dissipation to occur at magnetic null points this result predicts an observable relationship between flux imbalance and the amplitude and distribution of dissipation.

## I. INTRODUCTION

The process of magnetic reconnection has been proposed to explain energy release in many astrophysical plasmas, including solar coronal activity from flares, coronal mass ejections, ambient coronal heating and X-ray bright points [1]. Magnetic null points, which are locations where the magnetic field vector vanishes, have played a significant role in models of magnetic reconnection from their earliest introduction [2–4]. In some models energy dissipation occurs at the null point itself while in others null points are linked to topological boundaries, separatrices, separators, and bald patches [5] where the dissipation occurs. In most models of the first kind, here called *null point reconnection models*, field gradients naturally steepen near the null point, thereby enhancing local current densities and leading to efficient ohmic dissipation of magnetic energy in the immediate vicinity of the null [6–9]. In the second kind of models, here called *separator reconnection models*, dissipation results from an electric field along a separator field line [10, 11], defined as a field line connecting a pair of magnetic nulls. Most models of reconnection currently being investigated fall into one of these two categories and at present there is little observational evidence clearly favoring one over the other.

This lack of observational discrimination persists in spite of ample data from energetic solar coronal processes. The basic problem is the difficulty of applying specific reconnection models to the complicated magnetic geometries observed in the actual solar coronal field. Since null point reconnection models are inherently local they may be most easily applied, however, it is first necessary to locate null points in the coronal magnetic field. In this work we begin a more subtle approach to this problem: we determine which kinds of fields contain the

greatest number of coronal nulls and plan to seek evidence for more energy dissipation in them. Our first step will be to determine the number of coronal null points in a given magnetic field.

Even for the simplest method of field reconstruction, potential extrapolation, little is presently known about how many null points a field would have or how they would be distributed. A magnetic active region is a localized ( $\sim 100,000$  km) concentration of flux on the solar surface. Sufficiently far from the concentration a potential extrapolation can be approximated by its dipole and quadrupole terms (assuming that the region has no monopole moment). Such a far field will vanish at no more than two points at typical distances comparable to the horizontal scale of the flux distribution. It is less clear how many null points might exist in the region's near field, where a multipole expansion is inapplicable.

The very low corona is dominated by small-scale structures in the photospheric field and is affected less by the global active region configuration. The local photospheric structure will doubtless vary from region to region, however, it might be statistically similar among certain classes of regions, such as bipolar regions of similar age. Thus it is reasonable to look for a generic null-point distribution within the lowest layer of the coronal field. In particular, the potential field above an infinite distribution of photospheric flux which is statistically homogeneous, will have a well defined average density of null points. This particular null point density,  $\rho_N(z)$ , presented in this work, falls off so rapidly with height that it is safe to say that almost all coronal nulls are found in this layer.

The quiet Sun field is built from numerous small photospheric flux elements lying along the supergranular network. These elements are of mixed polarity, although there is often a dominant sign so that the large-scale

field appears unipolar. The local interconnections between opposing elements has been dubbed the *magnetic carpet* [12]. Reconnection within the magnetic carpet has been proposed as the mechanism which heats the quiet Sun corona [12–15] and accelerates the fast solar wind [16]. It is likely that the density of coronal null points depends in some way on the degree of flux imbalance. In the extreme case when all sources are of the same sign, the vertical field is always of that same sign and there can be no coronal nulls at all. One test of these theoretical models would be to compare the observed heating rates between quiet Sun regions of differing flux imbalances.

The distribution of magnetic null points above a perfectly balanced distribution of quiet Sun flux elements was studied numerically by Schrijver and Title [17]. They randomly distributed equal numbers of positive and negative point sources within a square region and numerically located all null points in the resulting potential field. Repeating this process for 200 realizations they found a density of null points scaling with the density of sources: there were  $0.093 \pm 0.003$  coronal nulls per source. They fit the distribution to a decreasing exponential of height over the limited range present in their experiments.

Albright developed a more general theory of null point distribution in random magnetic fields [18]. This theory is powerful enough to apply to a field of any spectrum, however, it assumes the statistics of the magnetic field are homogeneous and isotropic. This assumption makes the theory inapplicable to the solar coronal field whose spectrum is generally believed to soften with distance from its lower boundary, the photosphere. We present a generalization of Albright’s method to potential magnetic fields anchored to random boundary fields. The statistics of these boundary fields (photospheric fields) will be homogeneous and isotropic within the plane. Being potential extrapolations, the coronal fields will naturally vary with height and are neither homogeneous nor isotropic.

Our new method produces an analytic expression for the density of null points for specified photospheric-field statistics. The density is found to scale with the inverse cube of the field’s characteristic length at a given height. In a potential field this length scale increases monotonically with height, so the null density therefore decreases rapidly with height.

Magnetic null points in a three-dimensional field can be classified into two types: positive and negative (or B-type and A-type) [19, 20]. Our model makes further predictions concerning the distributions of each type of null. Sufficiently far from the surface all coronal nulls are of the sign opposite to the majority photospheric flux, while in a balanced photospheric distribution the two types of nulls are balanced.

We apply our general results to a model of the quiet Sun in which discrete flux elements are distributed at random. If the polarities are perfectly balanced the null density is self-similar above a certain height:  $\rho_N(z) \sim z^{-3}$ . This self-similar distribution is, however, not generic since any imbalance leads to a functional form describ-

ing a layer of nulls. This finding quantifies the assertion above that the density of coronal null points will depend on the degree of imbalance. We find that a distribution of elements will have coronal nulls only for balances more even than roughly 80% : 20%. We also find that the total number of null points within the layer actually increases with imbalance, reaching its peak at the 80% : 20% ratio.

The next section presents the analytic calculation of null point density in a potential magnetic field. In section 3 we apply the results to a model of the quiet Sun field composed of discrete photospheric sources. The resulting expression depends only slightly on the distribution of flux magnitudes and depends critically on the degree of imbalance. We verify our analytic expressions using Monte Carlo calculations similar to those of Schrijver and Title [17]. Finally we discuss the relevance of these results to models of coronal energetics.

## II. NULL POINT DISTRIBUTION

The spatial density of null points in a random vector field  $\mathbf{B}(\mathbf{x})$  is given by the expression derived by Albright (1999) and reviewed in Appendix A,

$$\rho_N = \langle \delta(\mathbf{B}) | \det(\partial B_i / \partial x_j) | \rangle , \quad (1)$$

where the average is over realizations of the field  $\mathbf{B}(\mathbf{x})$  and its derivative matrix  $\partial B_i / \partial x_j$ .

We consider a magnetic field  $\mathbf{B}(\mathbf{x})$  subject to a boundary condition prescribing its vertical component at a plane representing the photosphere ( $z = 0$ ),

$$B_z(\mathbf{x}_\perp, z=0) = b(\mathbf{x}_\perp) , \quad (2)$$

where  $\mathbf{x}_\perp = (x, y)$  denotes the horizontal coordinates. We take the coronal field to be the current-free field satisfying this boundary condition. This unique solution, the so-called potential field, may be computed from the Fourier transform of the photospheric field,  $\hat{b}(\mathbf{k})$ ,

$$\hat{b}(\mathbf{k}) \equiv \frac{1}{(2\pi)^2} \int b(\mathbf{x}_\perp) e^{-i\mathbf{k}\cdot\mathbf{x}_\perp} d\mathbf{x}_\perp ,$$

where the wave-vector  $\mathbf{k} = (k_x, k_y)$  has only horizontal components. The vertical and horizontal components of the extrapolated field are

$$B_z(\mathbf{x}_\perp, z) = \int \hat{b}(\mathbf{k}) e^{-|\mathbf{k}|z} e^{i\mathbf{k}\cdot\mathbf{x}_\perp} dk_x dk_y \quad (3)$$

$$\mathbf{B}_\perp(\mathbf{x}_\perp, z) = \int \frac{-i\mathbf{k}}{|\mathbf{k}|} \hat{b}(\mathbf{k}) e^{-|\mathbf{k}|z} e^{i\mathbf{k}\cdot\mathbf{x}_\perp} dk_x dk_y . \quad (4)$$

We consider an ensemble of photospheric fields  $b(\mathbf{x}_\perp)$  characterized by homogeneous and isotropic statistics. Here homogeneity and isotropy refer to properties within the  $(x, y)$  plane, on which the function  $b(\mathbf{x}_\perp)$  is defined. The statistics of the extrapolated field  $\mathbf{B}(\mathbf{x}_\perp, z)$

will vary along the vertical coordinate  $z$ . Assuming two-dimensional homogeneity and isotropy the statistics of the Fourier coefficients take the form

$$\langle \hat{b}(\mathbf{k}) \rangle = \bar{B} \delta(\mathbf{k}) \quad (5)$$

$$\langle \hat{b}(\mathbf{k}) \hat{b}^*(\mathbf{k}') \rangle - \bar{B}^2 \delta(\mathbf{k}) \delta(\mathbf{k}') = S(k) \delta(\mathbf{k} - \mathbf{k}') \quad (6)$$

where the function  $S(k)$  is the power spectrum of the photospheric magnetic field. Equation (5) admits the possibility of unbalanced flux over the entire photosphere, leading to a net vertical field. This allows regions with flux imbalance to be modeled, even though these cannot actually cover the entire solar surface.

The statistics of the potential magnetic field are related to the statistics of the photospheric field. The mean field

$$\langle \mathbf{B} \rangle = \bar{B} \hat{\mathbf{z}} \quad (7)$$

is purely vertical and does not vary with height. The variance of  $B_z$  depends on the photospheric spectrum

$$\langle B_z^2 \rangle - \bar{B}^2 \equiv \sigma^2(z) = 2\pi \int_0^\infty k S(k) e^{-2zk} dk \quad (8)$$

and is a non-increasing function of height. The moments of the other two components are equal,

$$\langle B_x^2 \rangle = \langle B_y^2 \rangle = \frac{1}{2} \sigma^2 \quad (9)$$

A complete list of all first and second moments is given in Appendix B. This list shows that the three components are mutually uncorrelated:  $\langle B_i B_j \rangle = 0$  for  $i \neq j$ .

To calculate the density of null points it is also necessary to determine the statistics of the derivative matrix  $M_{ij} = \partial B_i / \partial x_j$ . The matrix is symmetric,  $M_{ij} = M_{ji}$ , since the magnetic field has been assumed current-free. The mean of each matrix element vanishes, and their second moments can all be scaled to  $\langle M_{zz}^2 \rangle$  (see Appendix B). This moment will be written

$$\langle M_{zz}^2 \rangle \equiv q^2(z) \sigma^2(z) = 2\pi \int_0^\infty k^3 S(k) e^{-2kz} dk \quad (10)$$

introducing the inverse length scale  $q(z)$  which will turn out to play a fundamental role in the theory.

The magnetic field is divergence-free, so the matrix  $M_{ij}$  is traceless, and thus there are only two statistically independent variables between  $M_{xx}$ ,  $M_{yy}$  and  $M_{zz}$ . We will use  $M_{zz}$  and the statistically uncorrelated combination

$$M_\Delta \equiv M_{xx} - M_{yy} \quad (11)$$

as our representation of these two. The moment of this and the off-diagonal matrix elements follow from the assumption of isotropy, and are listed in Appendix B.

There are only three non-vanishing correlations among the eight variables  $B_x, B_y, B_z, M_{zz}, M_\Delta, M_{xy}, M_{xz}$  and  $M_{yz}$ , as shown in Appendix B. These include

$$\langle B_z M_{zz} \rangle = \frac{1}{2} \frac{d\sigma^2}{dz} = -2\pi \int_0^\infty k^2 S(k) e^{-2kz} dk \quad (12)$$

which will be expressed in terms of an anti-correlation coefficient

$$c \equiv - \frac{\langle B_z M_{zz} \rangle}{q \sigma^2} \quad (13)$$

defined to lie in the range  $0 \leq c \leq 1$ . The other two correlations are

$$\langle B_x M_{xz} \rangle = \langle B_y M_{yz} \rangle = -\frac{1}{2} q c \sigma^2 \quad (14)$$

### A. Gaussian fields

We have completely characterized the first and second moments of all eight random fields  $B_x, B_y, B_z, M_{zz}, M_\Delta, M_{xy}, M_{xz}$  and  $M_{yz}$ , in terms of the photospheric power spectrum  $S(k)$ . Unfortunately the null-density  $\rho_N(z)$  depends on moments beyond the first two. Indeed, it is not a simple function of any moments, depending as it does on  $|\det M_{ij}|$ . If we assume all fields are Gaussian, then the distributions of all fields are completely characterized by their first and second moments. Under this assumption it is possible to work out the null-density.

There are two independent random variables,  $M_\Delta$  and  $M_{xy}$ , and three pairs of correlated variables,  $(B_x, M_{xz})$ ,  $(B_y, M_{yz})$  and  $(B_z, M_{zz})$ . The probability distribution function  $p(\mathbf{B}, \mathbf{M})$  is therefore a simple product of five Gaussians. The independent variables are distributed as

$$p(M_\Delta) = \frac{1}{\sqrt{\pi} q \sigma} \exp \left[ -\frac{M_\Delta^2}{q^2 \sigma^2} \right] \quad ,$$

$$p(M_{xy}) = \frac{2}{\sqrt{\pi} q \sigma} \exp \left[ -\frac{4M_{xy}^2}{q^2 \sigma^2} \right] \quad .$$

The correlated pairs are distributed according according to two-dimensional Gaussians

---


$$p(B_x, M_{xz}) = \frac{1}{\pi \sigma^2 q \sqrt{1-c^2}} \times \exp \left[ -\frac{q^2 B_x^2 + 2qc B_x M_{xz} + M_{xz}^2}{\sigma^2 q^2 (1-c^2)} \right] \quad .$$

$$p(B_y, M_{yz}) = \frac{1}{\pi\sigma^2 q\sqrt{1-c^2}} \exp\left[-\frac{q^2 B_y^2 + 2qcB_y M_{yz} + M_{yz}^2}{\sigma^2 q^2 (1-c^2)}\right] .$$

$$p(B_z, M_{zz}) = \frac{1}{2\pi\sigma^2 q\sqrt{1-c^2}} \exp\left[-\frac{q^2 (B_z - \bar{B})^2 + 2qc(B_z - \bar{B})M_{zz} + M_{zz}^2}{2\sigma^2 q^2 (1-c^2)}\right] .$$

Performing the integrals of  $\delta(\mathbf{B}) d\mathbf{B}$  is equivalent to evaluating the joint functions at  $\mathbf{B} = 0$ . This results in reduced distributions for each of the correlated variables

$$p(0, M_{xz}) = \frac{1}{\pi\sigma^2 q\sqrt{1-c^2}} \exp\left[-\frac{M_{xz}^2}{\sigma^2 q^2 (1-c^2)}\right] .$$

$$p(0, M_{yz}) = \frac{1}{\pi\sigma^2 q\sqrt{1-c^2}} \exp\left[-\frac{M_{yz}^2}{\sigma^2 q^2 (1-c^2)}\right] .$$

$$p(0, M_{zz}) = \frac{e^{-\frac{1}{2}\bar{B}^2/\sigma^2}}{2\pi\sigma^2 q\sqrt{1-c^2}} \exp\left[-\frac{(M_{zz} - qc\bar{B})^2}{2\sigma^2 q^2 (1-c^2)}\right] .$$

We shall express each random variable  $M_{ij}$  in terms of a dimensionless random variable  $n_\ell$ ,

$$M_\Delta = q\sigma n_1/\sqrt{2} \quad (15)$$

$$M_{xy} = q\sigma n_2/\sqrt{8} \quad (16)$$

$$M_{xz} = q\sigma\sqrt{1-c^2}n_3/\sqrt{2} \quad (17)$$

$$M_{yz} = q\sigma\sqrt{1-c^2}n_4/\sqrt{2} \quad (18)$$

$$M_{zz} = q\sigma[\sqrt{1-c^2}n_5 + c\bar{B}/\sigma] . \quad (19)$$

Placing these in the probability density functions show that each  $n_\ell$  is distributed normally: it has zero mean and unit variance. The five normal variables are independent of one another.

Using definitions (15) – (19) in the determinant of expression (1) and performing the averages gives a simple version of the null density

$$\rho_N(z) = q^3(z) G(\bar{B}/\sigma, c) , \quad (20)$$

in terms of a dimensionless function of two variables. This function is

$$G(\zeta, c) \equiv \frac{e^{-\zeta^2/2}}{\sqrt{2\pi^{3/2}}} \left\langle \frac{1}{4} \left| (\sqrt{1-c^2}n_5 + c\zeta)^3 + [(1-c^2)(n_3^2 + n_4^2) - \frac{1}{2}(n_1^2 + n_2^2)] (\sqrt{1-c^2}n_5 + c\zeta) \right. \right. \\ \left. \left. + (1-c^2)[\sqrt{2}n_2n_3n_4 + \frac{1}{\sqrt{2}}(n_3^2 - n_4^2)n_1] \right| \right\rangle_{\mathbf{n}} ,$$

where the average is over the five uncorrelated normal variables  $n_1, \dots, n_5$ . The factor of  $q^3$  in expression (20) shows that the mean separation between nulls scales inversely with the length on which the field is structured.

The function  $G(\zeta)$  is even in  $\zeta$  and decreases rapidly for large values of  $|\zeta|$  as  $G \rightarrow 0.03 c^3 |\zeta|^3 e^{-\zeta^2/2}$ . This decrease reflects the fact that nulls are rare when the vertical magnetic field varies about a mean,  $\bar{B}$ , which is many standard deviations from zero. Graphs of the function  $G(\zeta, c)$  are given in fig. 1.

## B. Distributions of null types

Nulls can be classified as either positive or negative (also called B-type or A-type respectively) according to the sign of  $-\det(\partial B_i/\partial x_j)$  [19, 20]. The difference in their respective densities has a form, derived in Appendix A, which is the same as that for  $\rho_N$  but without the absolute values inside the average

$$\rho_N^+ - \rho_N^- = - \langle \delta(\mathbf{B}_0) \det(\mathbf{M}_0) \rangle . \quad (21)$$

Following the same steps we can evaluate the density difference for the case of Gaussian fields

$$\rho_N^+(z) - \rho_N^-(z) = -q^3(z) G_\Delta(\bar{B}/\sigma, c) , \quad (22)$$

where the dimensionless function  $G_\Delta$  is defined as  $G$ , both without the absolute values,

$$G_\Delta(\zeta, c) = \frac{e^{-\zeta^2/2}}{4\sqrt{2\pi^{3/2}}} c\zeta [(4-c^2) + c^2\zeta^2] . \quad (23)$$

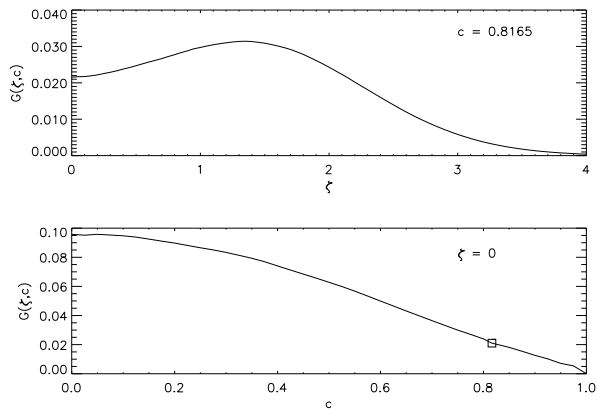


FIG. 1: Graphs of  $G(\zeta, c)$ . Top:  $G$  vs.  $\zeta$  for  $c = \sqrt{2/3}$ . Bottom:  $G$  vs.  $c$  for  $\zeta = 0$ . A square represents the point  $c = \sqrt{2/3}$ .

This difference density is odd in  $\zeta$ , and therefore vanishes when  $\zeta = 0$ , i.e. when  $\bar{B} = 0$ . Since  $0 \leq c \leq 1$  expression (23) always has the same sign as  $\zeta$ , meaning that the majority of nulls have the sign *opposite* to that of  $\bar{B}$ .

The ratio of the density difference to  $\rho_N$  is given by the ratio  $-G_\Delta/G$ . This ratio asymptotes to  $-\text{sgn}(\zeta)$  for  $|\zeta| \gg 1$ . This means that when  $|\bar{B}| \gg \sigma$  the few nulls present are almost exclusively positive (negative) when  $\bar{B} < 0$  ( $\bar{B} > 0$ ).

### III. THE QUIET SUN: A POISSON SOURCE DISTRIBUTION

A simple method for generating random homogeneous, isotropic fields  $b(\mathbf{x}_\perp)$  is to distribute point sources randomly with a density  $N$  [13]. Denoting the position and flux of source  $j$  by  $\mathbf{x}_j = (x_j, y_j)$  and  $\phi_j$  yields

$$b(\mathbf{x}_\perp) = \sum_j \phi_j \delta(\mathbf{x}_\perp - \mathbf{x}_j) . \quad (24)$$

The Fourier transform of this field yields statistical moments

$$\bar{B} = N \langle \phi_j \rangle , \quad S(k) = (2\pi)^{-2} N \langle \phi_j^2 \rangle , \quad (25)$$

where we have assumed that the flux  $\phi_j$  and location  $\mathbf{x}_j$  are independent random variables. Not surprisingly we find that a collection of photospheric point sources has a flat power spectrum  $S(k)$ .

We will assume that a source is positive with probability  $f$ , and that the magnitudes of positive and negative sources are identically distributed. Under this assumption the flux may then be written as

$$\phi_j = s_j \psi_j , \quad (26)$$

where  $s_j = \pm 1$  defines the polarity of the flux element and  $\psi_j > 0$  its magnitude. In terms of the magnitude

distribution we find

$$\langle \phi_j \rangle = (2f - 1)\bar{\psi} , \quad \langle \phi_j^2 \rangle = \langle \psi_j^2 \rangle . \quad (27)$$

Throughout this work we use two simple magnitude distributions for the illustration purposes. Little is known about the true distribution of the smallest elemental flux tubes, so we consider both a uniform and an exponential distribution. In a uniform distribution  $\psi_j = \bar{\psi}$  for all elements, while in an exponential distribution  $p(\psi_j) = \bar{\psi}^{-1} \exp(-\psi_j/\bar{\psi})$ . These two distributions have second moments  $\langle \psi_j^2 \rangle = \bar{\psi}^2$  or  $\langle \psi_j^2 \rangle = 2\bar{\psi}^2$  respectively.

The moments of the photospheric field lead immediately to the functions

$$\sigma^2 = \frac{\langle \psi_j^2 \rangle N}{8\pi z^2} \quad (28)$$

$$q = \sqrt{3/2} z^{-1} \quad (29)$$

$$c = \sqrt{2/3} . \quad (30)$$

The divergence in  $\sigma$  as  $z \rightarrow 0$  results from the use of point sources on the photosphere. Replacing the points with smooth profiles of width  $R$  will prevent this divergence. Nevertheless, at heights  $z \gg R$  the function  $S(k)$  becomes indistinguishable from that of point sources, and the result is the same. As we show below, this is the only regime in which the expression of  $\sigma(z)$  can be used to calculate the density of nulls.

#### A. The Gaussian Regime

Equation (20) depends on the assumption that the random fields have Gaussian distribution. At very low heights we expect the magnetic field to be dominated by the contribution from the nearest source and not to be Gaussian. A source at a horizontal distance  $r_1$  contributes

$$B_{1z} = \frac{\phi_1}{2\pi} \frac{z}{(r_1^2 + z^2)^{3/2}} \quad (31)$$

to the vertical field  $B_z$ . The distribution of the nearest-neighbor distance in a Poisson distribution of points [21]

$$p(r_1) = 2\pi N r_1 e^{-\pi N r_1^2} , \quad (32)$$

determines the distribution of  $B_{1z}$  which is therefore not Gaussian.

In a balanced field,  $f = 1/2$ , the fractional variance due to the nearest neighbor is

$$\frac{\langle B_{1z}^2 \rangle}{\langle B_z^2 \rangle} = 2e^{\pi N z^2} E_3(\pi N z^2) , \quad (33)$$

where  $E_3$  is the exponential integral. As  $z \rightarrow 0$  this ratio goes to unity; the nearest neighbor accounts for all of the field's variance. On the other hand, for  $z \geq 2N^{-1/2}$  the nearest point contributes less than 1/6 of the variance.

The remaining variance arises from uncorrelated contributions from at least five other sources. The central limit theorem holds that, under certain conditions, a sum of many independent terms will approximate a Gaussian variable. Thus we expect that at heights  $z \gtrsim 2N^{-1/2}$  all of the fields, including  $B_z$ , can be approximated by Gaussian distributions. Figure 2 verifies that the distribution of  $B_z$  is well-approximated by a Gaussian at  $z = 2N^{-1/2}$ , but not at much lower heights.

The ratio  $\bar{B}/\sigma$  increases linearly with height as  $z/h$  where the length scale is

$$h = \frac{\langle \psi^2 \rangle^{1/2}}{\bar{\psi}} \frac{N^{-1/2}}{\sqrt{8\pi|2f-1|}} . \quad (34)$$

The ratio  $\bar{B}/\sigma = \pm z/h$  where the sign depends on the sign of  $\bar{B}$ . Since  $G$  is even in its argument it is not necessary to distinguish between positive and negative cases.

The length scale  $h$  depends on the degree of flux imbalance, and goes to infinity for perfect balance:  $f = 1/2$ . The pre-factor  $\langle \psi^2 \rangle^{1/2}/\bar{\psi}$  will be 1 or  $\sqrt{2}$  for a uniform or exponential distribution of magnitudes. In terms of the height scale  $h$  the density of magnetic nulls takes the simple form

$$\rho_N(z) = (3/2)^{3/2} z^{-3} G(z/h, \sqrt{2/3}) . \quad (35)$$

In the case of perfectly balanced fluxes,  $f = 1/2$ , the mean field vanishes so the only relevant value is  $G(0, \sqrt{2/3}) \simeq 0.0217$ . This leads to a scale-invariant form of the the density of magnetic nulls

$$\rho_N = 0.040 z^{-3} , \quad (36)$$

regardless of the density of flux elements or the distribution of their magnitudes.

The graph of  $G(\zeta, \sqrt{2/3})$  in fig. 1 shows its value to drop rapidly beyond  $\zeta \simeq 3.0$ . Using expression (34) this means that most of the nulls are confined to a layer

$$z \lesssim \frac{\langle \psi^2 \rangle^{1/2}}{\bar{\psi}} \frac{3N^{-1/2}}{\sqrt{8\pi|2f-1|}} . \quad (37)$$

If this level is below the Gaussian regime,  $z \gtrsim 2N^{-1/2}$  then the analytic expression for null density predicts very few nulls. This means that significant null densities in the far-field occur only for

$$|2f-1| \lesssim \frac{\langle \psi^2 \rangle^{1/2}}{\bar{\psi}} \frac{3}{4\sqrt{2\pi}} . \quad (38)$$

For uniform or exponential magnitude distributions, a layer of nulls will occur above the plane for fractions in the range  $0.29 \lesssim f \lesssim 0.71$  or  $0.20 \lesssim f \lesssim 0.80$  respectively. This layer will be thinnest at the extremes, and be essentially infinite at  $f = 1/2$ .

There will be no coronal nulls above perfectly unipolar distributions,  $f = 1$  or  $f = 0$ , since  $B_z$  will be uniformly positive or negative respectively. This does not agree

with expression (20), which is always non-zero. The discrepancy arises because a  $B_z$  composed of random contributions of only one sign cannot be approximated, in the vicinity of  $B_z = 0$ , as a Gaussian variable.

Integrating  $\rho_N(z)$  downward from infinity gives the column density of nulls above a given height  $N_N(z)$ . The same function gives the number of nulls per source, when it is divided by the surface density of sources  $N$ . Figure 3 shows the columns for various flux imbalances,  $f \geq 0.5$ ; the curve for a given  $f$  applies to a flux imbalance of  $1-f$  as well. It is clear from these curves that the distribution of null points is more tightly confined for greater flux imbalances. Below a height of  $z \simeq 0.5$  ( $z = 1.0$ ) for a uniform (exponential) magnitude-distribution the flux imbalance makes little difference in the total column. Since these levels are below that where the Gaussian regime is applicable it is unclear how the observation might apply to the actual column density of nulls.

## B. The Non-Gaussian layer

In the layer immediately adjacent to the photosphere the Gaussian approximation does not apply. The magnetic field in this layer, defined by (37), is dominated by a few nearby sources. This means that the components of the magnetic field will not follow a Gaussian distribution, and will not be completely independent of one another. The results of section II A therefore do not apply. The derivation of the basic expression of null densities, (1), provided in Appendix A, makes no assumption about the statistics of the magnetic field, so it remains valid even in the Non-Gaussian layer.

To calculate the null density without assuming Gaussian statistics it is necessary to estimate the mean of  $\delta(\mathbf{B})|\det(\partial B_i/\partial x_j)|$  numerically. We make such estimates using the Monte-Carlo technique. We generate a realization of the random sources locations  $\mathbf{x}_j$  and fluxes  $\phi_j$ . The locations are generated randomly to populate a disk of radius  $r = R = 10$  with an average density of  $N = 1$ . Beginning at the center of the disk the radius  $r_1$  of the nearest neighbor is drawn from distribution (32). The radii of successively distant points,  $r_j$ , are then generated by drawing by drawing from the distribution

$$p(r_j) = 2\pi N r_j e^{-\pi N(r_j^2 - r_{j-1}^2)} , \quad j = 2, 3, \dots . \quad (39)$$

This is repeated until the final point  $r_n > R$  the radius of the disk. Thus the number of points in the disk is itself a random number, but will naturally have a mean  $\pi R^2/N = 314.16$ . Angular coordinates are generated for each point drawing from a uniform distribution of  $[0, 2\pi)$ . The magnetic flux of each source  $\phi_i$  is generated by drawing its magnitude  $\psi_i$  from the appropriate distribution (exponential or uniform) and a sign is generated randomly such that  $s_i = +1$  with a probability  $f$ .

For a given distribution of sources, designated by the index  $s$ , the field magnitude  $B_s = |\mathbf{B}|$  and Jacobi matrix

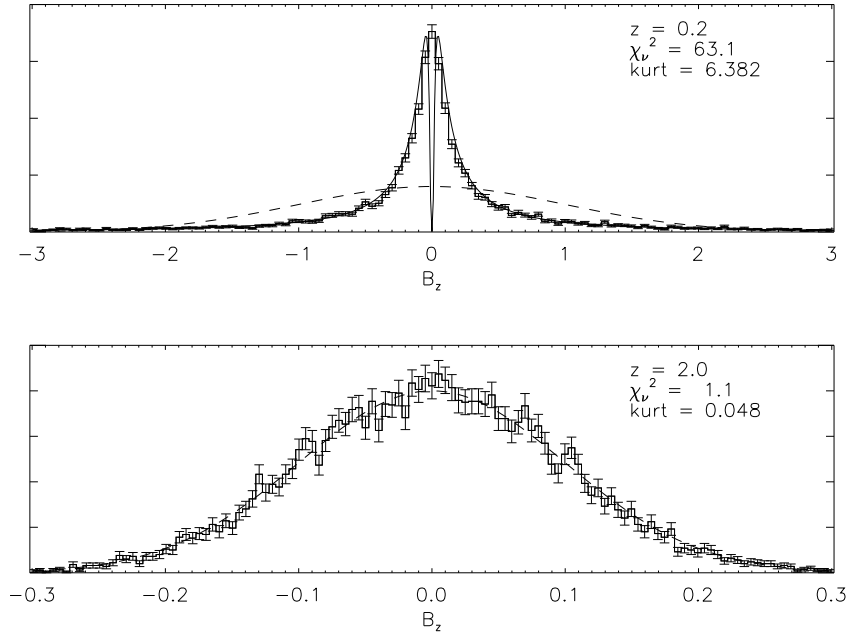


FIG. 2: Histograms of  $B_z$  from 10,000 realizations of a balanced ( $f = 1/2$ ) distribution of point sources with uniform magnitudes at a mean density of  $N = 1$ . Top: At  $z = 0.2N^{-1/2}$  the histogram does not fit a Gaussian (dashed curve); its kurtosis = 6.38 and  $\chi^2_\nu = 63.9$ . The curve does match the theoretical distribution of  $B_{1z}$ , the vertical field from the single nearest source (solid curve). Bottom: At  $z = 2N^{-1/2}$  the histogram is well fit by a Gaussian with  $\chi^2_\nu = 1.1$  (dashed curve); the data has kurtosis = 0.05.

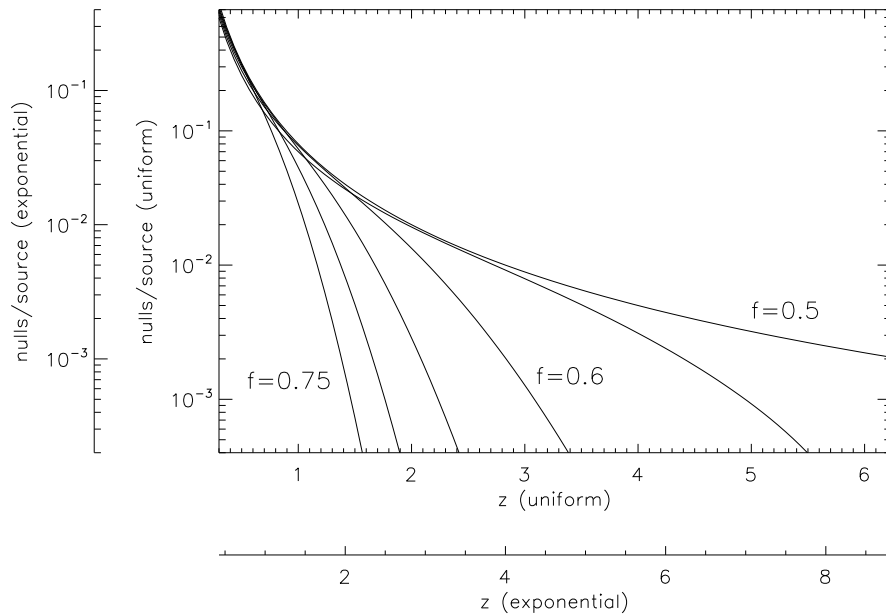


FIG. 3: The number of nulls per source above a given height  $z$  (in units of  $N^{-1/2}$ ). The six solid curves correspond to flux imbalances  $f = 0.5, 0.55, 0.6, 0.65, 0.7,$  and  $0.75$  reading roughly from right to left. The same curves also apply to  $f = 0.5, 0.45, 0.4, 0.35, 0.3,$  and  $0.25$ . The inner set of axes are the values for sources of uniform magnitude, while the outer axes apply to sources whose magnitude is distributed exponentially. The curves are found using analytic expressions which assume Gaussian fields, and thus do not apply much below  $z = 2$ .

determinant,  $D_s = \det(\partial B_i / \partial x_j)$  are evaluated at  $\mathbf{x} = (0, 0, z)$ , directly above the disk center. This is done for  $\mathcal{N} = 10,000$  different source distributions to generate a sampling of these quantities. As mentioned in Appendix A, the Dirac- $\delta$  function in (20) may be replaced by any function with unit integral and relatively local support. We use a Gaussian whose width,  $\Delta B = 0.25\sigma$ , is large enough to include a significant number of sample points. Our estimate of the null density is then

$$\rho_N(z) \simeq \frac{1}{\mathcal{N}} \sum_{s=1}^{\mathcal{N}} \frac{\exp[-\frac{1}{2}(B_s/\Delta B)^2]}{(\sqrt{2\pi}\Delta B)^3} |D_s|. \quad (40)$$

The field strength and matrix determinant can be evaluated at several heights using the same source distribution. Applying expression (40) independently to values from each realization gives the height dependence of  $\rho_N$ , shown for  $f = 1/2$  in fig. 4.

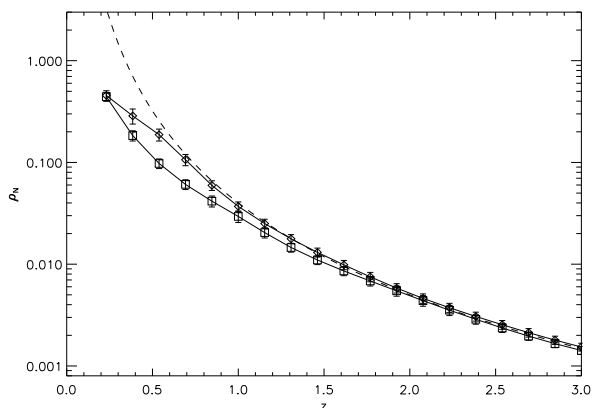


FIG. 4: The null density  $\rho_N(z)$  for balanced ( $f = 1/2$ ) flux distributions with density  $N = 1$ , found using the Monte Carlo integral (40). Diamonds are for a uniform distribution, squares for an exponential distribution. Error bars show  $3\sigma$  reflecting standard error in the mean (note that the different levels have errors which are not independent of one another).

The estimates above can be verified more directly by locating the null points within a sequence of sample magnetic fields. Random source distributions are generated within a disk of radius  $R = 10$ , exactly as described above. Null points in this field are found using a Newton-Raphson method from initial guesses. The initial guesses are generated randomly within the cylinder  $r < r_{\text{mx}} = 2.0$  and  $z < z_{\text{mx}} = 4.0$ . The search is performed with 5,000 initial guesses for each trial, and duplicate null points are discarded. To eliminate possible bias from the edge of the initial-guess cylinder, a histogram is generated from a cylinder inside it  $r < 1.75$ ,  $z < 3.0$ .

Figure 5 shows the null distributions found from  $\mathcal{N} = 3,000$  trials with a balanced ( $f = 1/2$ ) charge distribution both for uniform (left) and exponential (right) magnitude distribution. Both match well the analytic form (36), shown as a dashed curve, in the regime expected

to satisfy the assumption of Gaussian statistics,  $z \gtrsim 2$ . The true distribution is slightly lower than the analytic one even well below this level. This agrees with the independent calculation shown in fig. 4, which also shows that the exponential case departs more from the  $0.04z^{-3}$  behavior below  $z \simeq 1.5$ . Below  $z \simeq 0.5N^{-1/2}$  the actual distribution rolls over. This roll-over is notably absent from fig. 4, probably because the broadened  $\delta$ -function inevitably includes photospheric nulls in the coronal density at low levels; we describe below how much greater the density of photospheric nulls must be.

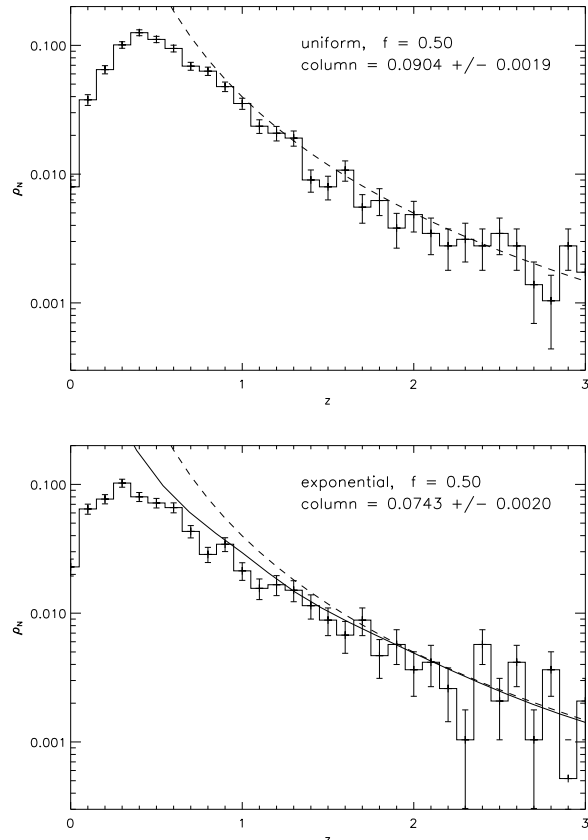


FIG. 5: The density of nulls for a balanced ( $f = 0.5$ ) distribution of point sources with uniform (top) and exponential (bottom) magnitude distributions. The solid curve, with error bars, show the results of a Monte-Carlo simulation. The dashed curve is the analytical prediction (36), and the solid line in the right panel is the results of the curve from fig. 4.

The total column of coronal nulls above an element of surface area  $N^{-1}$  is  $N_N = 0.090 \pm 0.002$  for uniform and  $N_N = 0.074 \pm 0.002$  for exponential magnitude distributions. The Gaussian approximation, (36), predicts this same column above  $z \simeq 1$  for both case (see fig. 3). Schrijver and Title found a slightly greater column,  $0.093 \pm 0.003$ , for source magnitudes distributed exponentially over a single decade; this distribution is intermediate between purely uniform and purely exponential [17]. It is possible that our gridless null-finding algorithm

misses some fraction of the coronal nulls, leading us to a systematically low column density. Undercounting appears to be small, however, as indicated by the statistical agreement of our histograms with the analytical prediction for  $z \gtrsim 1.5$ . On the other hand, Schrijver and Tittle use a spatial source-distribution differing from ours in several ways. Aside from their truncated exponential magnitude distribution they re-scale the magnitudes to assure perfect flux balance over their source-plane. Secondly, they search for nulls within a region whose horizontal extent is one-third of their source distribution, while ours is one-sixth. In any event, their finding and our uniform result agree on a column density of  $0.091$  at a level of one  $\sigma$ .

Null distributions above unbalanced source-distributions, such as the  $f = 0.7$  case shown in fig. 6a, reveal one unexpected tendency. They conform to expectation that both the uniform (left) and exponential (right) magnitude distributions produce nulls restricted to a narrower layer —  $z \lesssim 1.5$  and  $z \lesssim 2.0$ , respectively. Once again these fit the analytic predictions for  $z \gtrsim 1.5$ . Paradoxically, the total column in each case is greater than for balanced sources:  $N_N = 0.129 \pm 0.002$  (uniform) and  $N_N = 0.087 \pm 0.002$  (exponential). A plot of the column versus imbalance fraction  $f$ , shown in 7a, suggests that this trend continues to  $f \simeq 0.8$ : there are greater densities within narrower layers.

### C. Photospheric nulls

Magnetic fields generated by isolated photospheric sources will generally include a population of photospheric nulls. Outside of the sources,  $B_z = 0$  everywhere in the photosphere, so photospheric nulls will occur at isolated points where  $\mathbf{B}_\perp = 0$ . One method of identifying null points is to generate the magnetic field continuously by successively “turning on” each of the photospheric sources; that is to say increasing its net flux from zero to its final value  $\phi_j$ . At the instant a point source is first turned on, a single null appears on the photospheric plane next to it (except in the special case where the source is placed at the location of a pre-existing photospheric null). The sign of the null will always match the sign of the source. The location of the null will change continuously as the source’s flux increases.

During this continuous procedure it is possible for the null to undergo a discontinuous change known as a *bifurcation*. A curl-free vector field can undergo only two types of local bifurcations [22, 23]. In a *saddle-node* bifurcation two new nulls of opposing sign appear where none had existed before. In the inverse process an existing null “coalesces” with an opposing null and both disappear (also called a *local separator bifurcation* [24]). In a *pitchfork bifurcation* one null becomes three nulls, two of the same sign as the original and one of the opposite sign (in topological studies this has been dubbed a *double separator bifurcation* [25]). Such a bifurcation

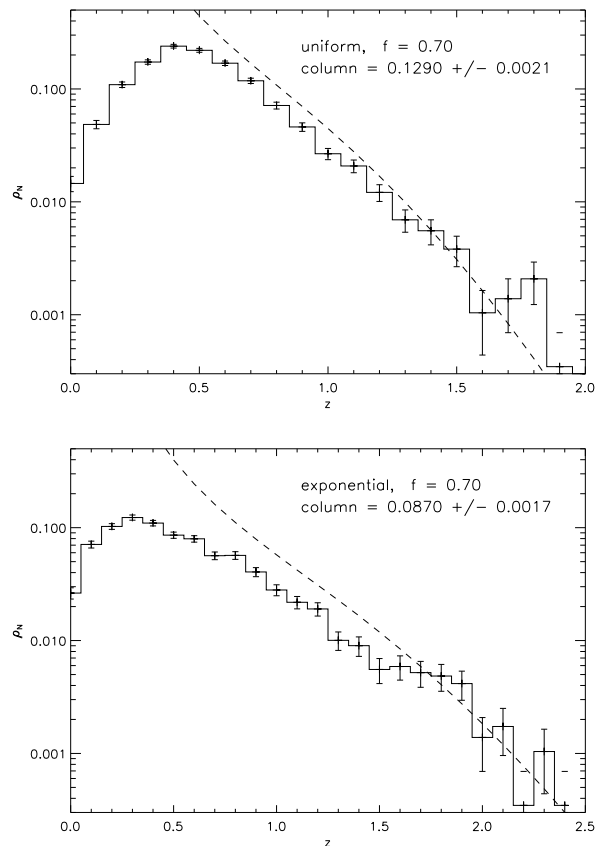


FIG. 6: The density of null points for unbalanced source distributions:  $f = 0.7$  with uniform (top) and exponential (bottom) magnitude distributions. The solid curve, with error bars, show the results of a Monte-Carlo simulation. The dashed curve is the analytical prediction (35).

requires a spatial symmetry, lest it degenerate into a saddle node bifurcation in the neighborhood of an existing null. Our field possesses one symmetry with respect to reflection through the  $z = 0$  plane. This means that, in general, pitchfork bifurcations will only occur vertically creating one coronal null and one null in the mirror corona ( $z < 0$ ). It also means that general saddle node bifurcations in the photosphere will be planar, producing only photospheric nulls.

Without bifurcation all nulls would be photospheric, and there would be one null per source (the actual number is one or two less than the number of sources, however, in our infinite system this difference is irrelevant). Therefore, the presence of coronal nulls shows that some bifurcations must occur during the hypothetical turn-on process. For an imbalanced source distribution,  $f \neq 1/2$ , the vast majority of nulls in the high corona ( $\zeta \gg 1$ ) are of one sign (opposite to that of the dominant source species). Since saddle node bifurcations create nulls of opposite sign in equal numbers, there must have been pitchfork bifurcations at the photospheric surface to give rise to coronal nulls of a predominant sign. The null cre-

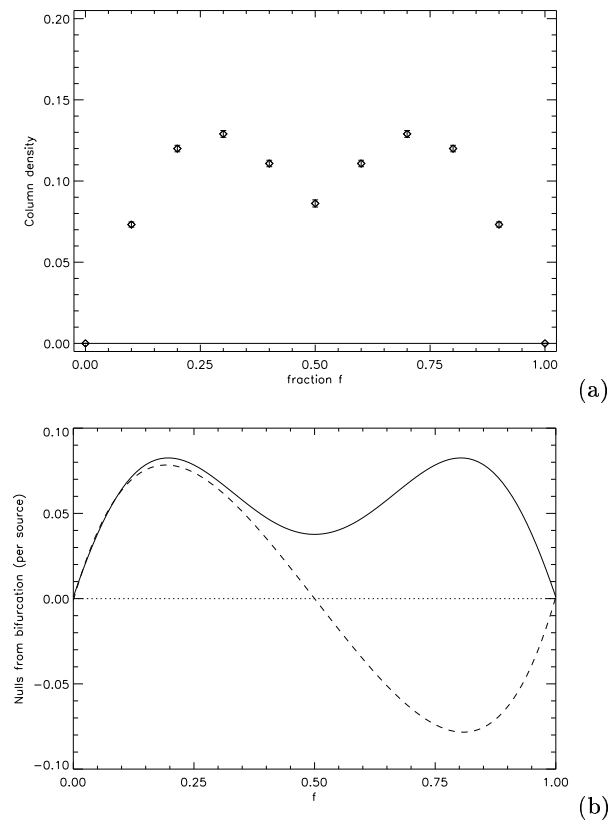


FIG. 7: The column of nulls  $N_N$  vs. imbalance fraction  $f$  for a uniform magnitude distribution found numerically (a) and predicted by bifurcation probability of photospheric nulls (b). Numerical results (a) shown with error bars are the total columns found from 2,000 trials. The bifurcation prediction (b) is the column of null points (solid) produced through pitchfork bifurcation during turn-on. Also shown (dashed) is the difference in column between positive and negative nulls. Results for an exponential distribution are similar.

ated at the instant of turn-on will be the same as that of the charge. If this null undergoes a pitchfork bifurcation it creates a coronal null of the same sign, and changes the sign of the photospheric null. The population of nulls in the high corona is consistent with the results of pitchfork bifurcations. Since we have also shown that the null points are preferentially of sign opposite to that of  $\bar{B}$ , they must arise from bifurcations of nulls from the minority species.

#### D. Probabilities of photospheric bifurcation

The foregoing discussion showed that coronal nulls can be related to bifurcations during a hypothetical turn-on process. If coronal nulls arose only through this process, then the total number of coronal nulls would equal the number of photospheric nulls times the probability of a given null undergoing bifurcation during a turn-on scenario. This probability can be estimated using Monte-

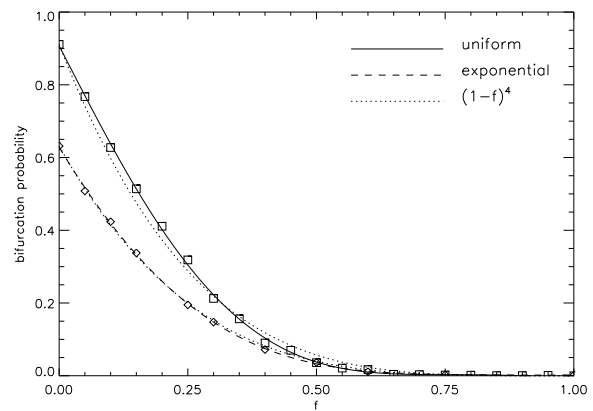


FIG. 8: The probability of a pitchfork bifurcation when a positive source is turned on among a distribution of other sources, of which a fraction  $f$  are positive. Magnitudes of sources have uniform (solid) or exponential (dashed) distributions. The data points from the Monte Carlo simulations are shown as squares and diamond respectively. Dotted curves show  $(1-f)^4 p_{\text{pb}}(0)$  for each of the two cases.

Carlo methods.

A random distribution of sources is generated, beginning from a central point, as described above. A final source is then placed at the very center,  $\mathbf{x} = 0$ . (This takes advantage of a well-known, but sometimes surprising property of Poisson processes: the distributions  $p(r_j)$  of successive radii apply equally to distances from a given source or from an arbitrary point in the plane.) The flux of this central source is then ramped continuously from zero to a positive value drawn from the same distribution as the other sources (uniform or exponential). The ramping is performed as a sequence of increases. After each increase the null is re-located using its previous location as an initial guess. When the new null is deemed to be too far from its previous location a smaller flux increase is attempted. This process is applied recursively to assure that each null is tracked continuously from its birth. As the null is tracked its type is monitored by noting the sign of  $-\det(\partial B_i / \partial x_j)$ . When the determinant changes sign a pitchfork bifurcation has occurred. This entire procedure is then repeated several thousand times to determine the probability of a pitchfork bifurcation,  $p_{\text{pb}}(f)$ .

The results of these simulations are shown in fig. 8 for both uniform and exponential distributions. In both cases, bifurcation is far more likely when turning on a charge whose sign is that of the minority. In the limit  $f \rightarrow 0$  the charge turned on is always surrounded by opposing sources and its null will bifurcate 91% (63%) of the time when the surrounding magnitudes are distributed uniformly (exponentially). Each curve is similar to  $(1-f)^4$  (dotted) suggesting that a source is most likely to bifurcate when its four closest neighbors are of opposite sign.

If each bifurcation is a forward bifurcation, producing a coronal null, then the total number of such coronal nulls per source is a weighted average of those from each of the two signs

$$N_N(f) = f p_{pb}(f) + (1-f) p_{pb}(1-f) . \quad (41)$$

The result, fig. 7b, shows how the rare bifurcations of the common species combine with the common bifurcations of the rare species. The optimal balance appears to be at  $f \simeq 0.2$  or  $f \simeq 0.8$ , when minorities are outnumbered by a factor four; four was empirically found to be the number of opposing sources needed for a bifurcation.

This theoretical curve is similar in shape, but roughly half the magnitude, of the numerically-determined approximation of the column densities shown in fig. 7a. The disagreement in magnitude leads us to conclude that most of the coronal nulls are not those arising through pitchfork bifurcation in a turn-on process.

The difference in columns of the two null types, due to photospheric saddle-node bifurcation, is

$$N_\Delta(f) = N_N^+ - N_N^- = f p_{pb}(f) - (1-f) p_{pb}(1-f), \quad (42)$$

since the bifurcation from a positive source yields a positive coronal null. Any subsequent bifurcations in the coronal field must preserve the Euler characteristic of this field, the difference between positive and negative nulls, and will therefore leave  $N_\Delta$  unchanged. The dashed curve in fig. 7b shows that when  $f > 1/2$  (and therefore  $\bar{B} > 0$ ), the difference  $N_\Delta$  is negative. Thus the predominant coronal nulls are of the same sign as the minority species. This matches the result of the Gaussian-field theory.

#### IV. DISCUSSION

We have found a general expression for the density of null points in the potential corona above a statistically

homogeneous distribution of photospheric field. The density scales inversely with the cube of the characteristic scale of the coronal magnetic field. Since this scale increases with height in any potential field, the density of nulls naturally decreases with height. If the photospheric field has a dominant sign of field, the nulls will be confined to a layer. Higher in this layer almost every null has a sign opposite to the sign of dominant flux.

In the case of photospheric field produced by localized sources we find that coronal nulls are quite rare; there are never more than thirteen per hundred sources. The null density is maximum at a height roughly one half the mean source separation. Above this the density falls quickly with height. As the photospheric sources are more evenly balanced the layer of nulls is thicker, but the total column of null points decreases. For perfectly balanced sources the nulls are distributed self-similarly as  $\rho_N \simeq 0.04z^{-3}$ , regardless of any other property of the source distribution. We find that a roughly 80% : 20% mixture of source signs produces the maximum number of nulls. These nulls are tightly confined to a layer whose thickness is the horizontal inter-source spacing.

#### Acknowledgments

The authors gratefully acknowledge the support of NASA grant NAG5-10489 and the Institute for Theoretical Physics where the work was conducted. The Institute for Theoretical Physics is supported by the National Science Foundation Under Grant No. PHY99-07949.

- 
- [1] E. R. Priest and T. G. Forbes, *Magnetic Reconnection. MHD theory and applications*, (Cambridge University Press, 2000).
  - [2] J. W. Dungey, *Cosmic Electrodynamics*, (Cambridge University Press, Cambridge, U.K., 1958).
  - [3] Y.-T. Lau and J. M. Finn, *Astrophys. J.* **350**, 672 (1990).
  - [4] K. Schindler and M. Hesse, *J. Geophys. Res.* **93**, 5547 (1988).
  - [5] V. S. Titov, E. R. Priest, and P. Demoulin, *Astron. Astrophys.* **276**, 564 (1993).
  - [6] S. V. Bulanov and M. A. Olshanetskii, *Phys. Lett.* **100A**, 35 (1984).
  - [7] I. J. D. Craig and A. N. McClymont, *Astrophys. J.* **371**, L41 (1991).
  - [8] A. B. Hassam, *Astrophys. J.* **399**, 159 (1992).
  - [9] V. S. Titov and E. R. Priest, *Geophys. Astrophys. Fluid Dynamics* **72**, 249 (1993).
  - [10] D. W. Longcope, *Solar Phys.* **169**, 91 (1996).
  - [11] K. Galsgaard and A. Nordlund, *J. Geophys. Res.* **102**, 231 (1997).
  - [12] C. J. Schrijver, A. M. Title, K. L. Harvey, J. Sheeley, N. R., Y.-M. Wang, G. H. J. van den Oord, R. A. Shine, T. D. Tarbell, and N. E. Hurlburt, *Nature* **394**, 152 (1998).
  - [13] D. W. Longcope and C. C. Kankelborg, *Astrophys. J.* **524**, 483 (1999).
  - [14] E. R. Priest, J. F. Heyvaerts, and A. M. Title, *Astrophys. J.* **576**, 533 (2002).
  - [15] E. R. Priest, D. W. Longcope, and V. S. Titov, *Astrophys. J.* (2003), (submitted).
  - [16] J. F. McKenzie, M. Banaszekiewicz, and W. I. Axford, *Astron. Astrophys.* **303**, L45 (1995).

- [17] C. J. Schrijver and A. M. Title, *Solar Phys.* **207**, 223 (2002).  
 [18] B. J. Albright, *Phys. Plasmas* **6**, 4222 (1999).  
 [19] S. W. H. Cowley, *Radio Sci.* **8**, 903 (1973).  
 [20] E. R. Priest, *Phys. Plasmas* **4**, 1945 (1996).  
 [21] M. G. Kendall and P. A. P. Moran, *Geometrical probability*, (Charles Griffin and Co., London, 1963).  
 [22] J. Guckenheimer and P. Holmes, *Nonlinear Oscillations, Dynamical Systems, and Bifurcations of Vector Fields*, (Springer-Verlag, New York, 1983).  
 [23] D. S. Brown and E. R. Priest, *Solar Phys.* **190**, 25 (1999).  
 [24] D. S. Brown and E. R. Priest, *Astron. Astrophys.* **367**, 339 (2001).  
 [25] E. R. Priest, T. N. Bungey, and V. S. Titov, *Geophys. Astrophys. Fluid Dynamics* **84**, 127 (1997).  
 [26] S. O. Rice, *Noise and Stochastic Processes*, edited by N. Wax, (Dover, New York, 1954), p. 133.

---

## APPENDIX A: DENSITY OF NULL POINTS

The density of null points in a random vector field  $\mathbf{B}(\mathbf{x})$  was derived by Albright [18] by generalizing a technique due to Rice [26]. Here we present a variation on this original derivation.

Consider a ball of radius  $\epsilon$  centered at a point  $\mathbf{x}_0$ . If  $\epsilon$  is small enough, the probability of finding a null within the ball is  $P_\epsilon \simeq \rho_N(\mathbf{x}_0)V$ , where  $V = (4/3)\pi\epsilon^3$ , is the volume of the ball. We assume that the radius  $\epsilon$  is also small enough that the magnetic field within the ball may be approximated by the first two terms in its Taylor series

$$\mathbf{B}(\mathbf{x}_0 + \delta\mathbf{x}) = \mathbf{B}_0 + \mathbf{M}_0 \cdot \delta\mathbf{x} \quad , \quad |\delta\mathbf{x}| \leq \epsilon \quad (\text{A1})$$

where  $\mathbf{B}_0 = \mathbf{B}(\mathbf{x}_0)$  and  $\mathbf{M}_0 = \mathbf{M}(\mathbf{x}_0)$  are a random vector and a random traceless symmetric matrix respectively. In this case it becomes possible to evaluate the probability  $P_\epsilon$  and to find  $\rho_N$  from this.

The condition for expression (A1) to vanish is that  $\mathbf{B}_0 = -\mathbf{M}_0 \cdot \delta\mathbf{x}$ , for some point  $\delta\mathbf{x}$  inside the ball. A given realization of the Jacobian matrix  $\mathbf{M}_0$  maps the sphere with volume  $V$  to an ellipsoid  $\mathcal{E}$  with volume  $|\det(\mathbf{M}_0)|V$ . There will be a null point within the ball if and only if the random vector  $\mathbf{B}_0$  falls inside the ellipsoid  $\mathcal{E}$ , centered at the origin  $\mathbf{B}_0 = 0$ . The probability that this occurs can be expressed in terms of the joint probability density function  $p(\mathbf{B}_0, \mathbf{M}_0)$  as

$$P_\epsilon = \int d\mathbf{M}_0 \int_{\mathcal{E}} d\mathbf{B}_0 p(\mathbf{B}_0, \mathbf{M}_0) \quad , \quad (\text{A2})$$

where the outer integral is over all Jacobian matrices  $\mathbf{M}_0$ , while the inner integral is restricted to  $\mathbf{B}_0 \in \mathcal{E}$ . For vanishingly small  $\epsilon$  the inner integral can be approximated

$$\begin{aligned} \int_{\mathcal{E}} d\mathbf{B}_0 p(\mathbf{B}_0, \mathbf{M}_0) &\simeq V |\det(\mathbf{M}_0)| p(\mathbf{0}, \mathbf{M}_0) \\ &= V \int d\mathbf{B}_0 p(\mathbf{B}_0, \mathbf{M}_0) |\det(\mathbf{M}_0)| \delta(\mathbf{B}_0) \quad . \end{aligned} \quad (\text{A3})$$

The Dirac- $\delta$  function in this expression could be replaced with any function of local support whose integral is unity. Broader support is desirable when trying to estimate the mean by an average over samples, since the variance of  $\delta(\mathbf{B})$  is infinite.

The density of null points at  $\mathbf{x}_0$  is defined as the probability per unit volume of finding a null point within a volume. Therefore

$$\begin{aligned} \rho_N(\mathbf{x}) &= \frac{P_\epsilon}{V} = \int d\mathbf{M}_0 \int d\mathbf{B}_0 p(\mathbf{B}_0, \mathbf{M}_0) |\det(\mathbf{M}_0)| \delta(\mathbf{B}_0) \\ &= \langle \delta(\mathbf{B}_0) | \det(\mathbf{M}_0) | \rangle \quad , \end{aligned} \quad (\text{A4})$$

where the average is defined integrating  $p(\mathbf{B}_0, \mathbf{M}_0)d\mathbf{B}_0d\mathbf{M}_0$  over all values of all fields. This expression makes no assumptions about the magnetic field or its statistics.

A positive (negative) null is one where  $\det(\mathbf{M})$  is negative (positive). Assuming that the sign of  $\det(\mathbf{M})$  at the null point is the same as  $\det(\mathbf{M}_0)$  we can calculate the probability of finding a positive/negative null inside the ball,  $P_\epsilon^\pm$ , by multiplying the probability density by the Heaviside function  $\Theta[\mp \det(\mathbf{M}_0)]$ . The integrand then contains the product

$$\Theta[\mp \det(\mathbf{M}_0)] |\det(\mathbf{M}_0)| = \frac{1}{2} |\det(\mathbf{M}_0)| \mp \frac{1}{2} \det(\mathbf{M}_0) \quad .$$

Thus the density of positive/negative nulls is given by

$$\rho_N^\pm(\mathbf{x}_0) = \frac{1}{2} \langle \delta(\mathbf{B}_0) | \det(\mathbf{M}_0) | \rangle \mp \frac{1}{2} \langle \delta(\mathbf{B}_0) \det(\mathbf{M}_0) \rangle \quad . \quad (\text{A5})$$

The difference in these densities is

$$\rho_N^+ - \rho_N^- = - \langle \delta(\mathbf{B}_0) \det(\mathbf{M}_0) \rangle , \quad (\text{A6})$$

can be seen to satisfy the inequality  $|\rho_N^+ - \rho_N^-| \leq \rho_N$ , so neither of the densities is negative.

## APPENDIX B: STATISTICS OF THE FIELDS

We must characterize the statistics of all eight variables  $B_x, B_y, B_z, M_{zz}, M_\Delta, M_{xy}, M_{xz}$  and  $M_{yz}$ , in terms of the statistics of the photospheric field  $b(\mathbf{x}_\perp)$ . The components of the magnetic field are expressed as inverse Fourier transforms

$$B_z(\mathbf{x}_\perp, z) = \int \hat{b}(\mathbf{k}) e^{-|\mathbf{k}|z} e^{i\mathbf{k}\cdot\mathbf{x}_\perp} dk_x dk_y \quad (\text{B1})$$

$$\mathbf{B}_\perp(\mathbf{x}_\perp, z) = \int \frac{-i\mathbf{k}}{|\mathbf{k}|} \hat{b}(\mathbf{k}) e^{-|\mathbf{k}|z} e^{i\mathbf{k}\cdot\mathbf{x}_\perp} dk_x dk_y . \quad (\text{B2})$$

Taking the average of (B1) and using eq. (5) yields

$$\langle B_z \rangle = \int \bar{B} \delta(\mathbf{k}) e^{-|\mathbf{k}|z} e^{i\mathbf{k}\cdot\mathbf{x}_\perp} dk_x dk_y = \bar{B} , \quad (\text{B3})$$

independent of  $z$ .

The first moments of the remaining seven variables vanish due to our assumption of planar-homogeneity. The horizontal fields may be written in terms of a scalar potential  $\chi(\mathbf{x})$  generated by  $b(\mathbf{x}_\perp)$ . In terms of this

$$\langle B_j \rangle = - \frac{\partial}{\partial x_j} \langle \chi \rangle , \quad j = 1, 2 . \quad (\text{B4})$$

The statistics of  $\chi$  will be homogeneous because that is true of  $b(\mathbf{x}_\perp)$ . Thus its average will not depend on  $x$  or  $y$ , and  $\langle B_x \rangle = \langle B_y \rangle = 0$ . The average of any element of the Jacobian matrix vanishes,

$$\langle M_{ij} \rangle = \frac{\partial}{\partial x_i} \langle B_j \rangle = 0 , \quad (\text{B5})$$

since each average  $\langle B_j \rangle$  is constant.

The complete set of second moments includes eight variances and twenty eight cross-correlations. To treat these generally we introduce the notation  $D_x \equiv B_x - \langle B_x \rangle$ ,  $D_\Delta \equiv M_\Delta - \langle M_\Delta \rangle$ ,  $D_{xy} \equiv M_{xy} - \langle M_{xy} \rangle$  and so forth. All means are subtracted for notational consistency, even though seven of the eight are zero. Recall that  $M_\Delta \equiv M_{xx} - M_{yy}$  is introduced to account for the fact that  $M_{xx} + M_{yy} + M_{zz} = 0$ . All eight functions can then be written in the form

$$D_\alpha(\mathbf{x}_\perp, z) = \int [\hat{b}(\mathbf{k}) - \bar{B}\delta(\mathbf{k})] \hat{D}_\alpha(\mathbf{k}) e^{-|\mathbf{k}|z} e^{i\mathbf{k}\cdot\mathbf{x}_\perp} dk_x dk_y , \quad (\text{B6})$$

where  $\alpha = x, y, \dots, yz, zz$  and the functions  $\hat{D}_\alpha(\mathbf{k})$  are found by inspection of (B1), (B2) or derivatives thereof; they are listed in table I. Using (6) gives the variance or cross-correlation as a spectral integral

$$\begin{aligned} \langle D_\alpha D_\beta \rangle &= \int S(k) \hat{D}_\alpha(\mathbf{k}) \hat{D}_\beta^*(\mathbf{k}) e^{-2|\mathbf{k}|z} dk_x dk_y \\ &= 2\pi \int_0^\infty S(k) \hat{D}_{\alpha\beta}(k) e^{-2kz} k dk , \end{aligned} \quad (\text{B7})$$

where the double-subscripted function  $\hat{D}_{\alpha\beta}(k)$  is defined by the angle-average

$$\hat{D}_{\alpha\beta}(k) \equiv \frac{1}{2\pi} \int_0^{2\pi} \hat{D}_\alpha(\mathbf{k}) \hat{D}_\beta^*(\mathbf{k}) d\theta_k . \quad (\text{B8})$$

Since each  $\hat{D}_\alpha$  is proportional to a single trigonometric function of  $\theta_k$  these integrals are easily evaluated (see table I). Basic properties of trigonometric functions make it evident that  $\hat{D}_{\alpha\beta} \neq 0$  only when  $\hat{D}_\alpha$  and  $\hat{D}_\beta$  are proportional

$\alpha$	$\hat{D}_\alpha(k, \theta_k)$	$\hat{D}_{\alpha\alpha}(k)$	$\beta$	$\hat{D}_{\alpha\beta}(k)$
$x$	$-i \cos \theta_k$	$\frac{1}{2}$	$xz$	$-\frac{1}{2}k$
$y$	$-i \sin \theta_k$	$\frac{1}{2}$	$yz$	$-\frac{1}{2}k$
$z$	$1$	$1$	$zz$	$-k$
$\Delta$	$k \cos 2\theta_k$	$\frac{1}{2}k^2$		—
$xy$	$\frac{1}{2}k \sin 2\theta_k$	$\frac{1}{8}k^2$		—
$xz$	$ik \cos \theta_k$	$\frac{1}{2}k^2$	$x$	$-\frac{1}{2}k$
$yz$	$ik \sin \theta_k$	$\frac{1}{2}k^2$	$y$	$-\frac{1}{2}k$
$zz$	$-k$	$k^2$	$z$	$-k$

TABLE I: A summary of the eight random fields.

to the same function of  $\theta_k$ . This happens when  $\alpha = \beta$ , which gives the variance, and for three other pairs of  $\alpha-\beta$ , namely  $x-xz$ ,  $y-yz$  and  $z-zz$ . These are then the only three correlations among twenty eight which do not vanish.

Table I shows that each of the functions  $\hat{D}_{\alpha\beta}(k)$  is a monomial in  $k$  of power not greater than two. Placing these in (B7) gives one of the three spectral integrals

$$2\pi \int_0^\infty k S(k) e^{-2kz} dk \equiv \sigma^2 \quad (\text{B9})$$

$$2\pi \int_0^\infty k^2 S(k) e^{-2kz} dk \equiv q^2 \sigma^2 \quad (\text{B10})$$

$$2\pi \int_0^\infty k^3 S(k) e^{-2kz} dk \equiv qc\sigma^2 \quad (\text{B11})$$

It can be seen that these integrals are related by

$$qc = -\frac{1}{2\sigma^2} \frac{\partial \sigma^2}{\partial z} \quad (\text{B12})$$

$$q^2 = \frac{1}{4\sigma^2} \frac{\partial^2 \sigma^2}{\partial z^2}, \quad (\text{B13})$$

so all properties of the fields depend on the Laplace transform of the photospheric power spectrum  $S(k)$ . Each of the averages  $\langle D_\alpha D_\beta \rangle$  is proportional to one of these with a factor given in table I. The complete set is

$$\begin{aligned} \langle B_x^2 \rangle &= \langle B_y^2 \rangle = \frac{1}{2}\sigma^2 \\ \langle B_z^2 \rangle &= \sigma^2 \\ \langle M_\Delta^2 \rangle &= \frac{1}{2}q^2\sigma^2 \\ \langle M_{xy}^2 \rangle &= \frac{1}{8}q^2\sigma^2 \\ \langle M_{xz}^2 \rangle &= \langle M_{yz}^2 \rangle = \frac{1}{2}q^2\sigma^2 \\ \langle M_{zz}^2 \rangle &= q^2\sigma^2 \\ \langle B_x M_{xz} \rangle &= \langle B_y M_{yz} \rangle = -\frac{1}{2}qc\sigma^2 \\ \langle B_z M_{zz} \rangle &= -qc\sigma^2 \end{aligned}$$


---